Optimal entanglement-assisted discrimination of quantum measurements

M. Miková,[1] M. Sedlák,[1,2] I. Straka,[1] M. Mičuda,[1] M. Ziman,[2,3] M. Ježek,[1] M. Dušek,[1] and J. Fiurášek[1]

[1]*Department of Optics, Palacký University, 17. listopadu 1192/12, CZ-771 46 Olomouc, Czech Republic*

[2]*RCQI, Institute of Physics, Slovak Academy of Sciences, Dúbravská cesta 9, 84511 Bratislava, Slovakia*

[3]*Faculty of Informatics, Masaryk University, Botanická 68a, 60200 Brno, Czech Republic*

(Received 14 April 2014; revised manuscript received 24 July 2014; published 15 August 2014)

We investigate optimal discrimination between two projective single-qubit measurements in a scenario where the measurement can be performed only once. We consider general setting involving a tunable fraction of inconclusive outcomes and we prove that the optimal discrimination strategy requires an entangled probe state for any nonzero rate of inconclusive outcomes. We experimentally implement this optimal discrimination strategy for projective measurements on polarization states of single photons. Our setup involves a real-time electrooptical feed-forward loop which allows us to fully harness the benefits of entanglement in discrimination of quantum measurements. The experimental data clearly demonstrate the advantage of entanglement-based discrimination strategy as compared to unentangled single-qubit probes.

DOI: 10.1103/PhysRevA.90.022317 PACS number(s): 03.67.Bg, 42.50.Dv, 42.50.Ex

I. INTRODUCTION

One of the characteristic traits of quantum mechanics is the impossibility to perfectly discriminate two nonorthogonal quantum states. This fundamental property of quantum systems has far reaching practical implications ranging from security of quantum key distribution protocols to limits on measurement precision in metrologic schemes. Impossibility of perfect discrimination also immediately triggers the question what is the optimal approximate or probabilistic discrimination strategy. Given their wide range of potential applications, such strategies have been studied in great detail both theoretically [1–11] and experimentally [12–16]. More recently, this concept has been extended to discrimination of quantum operations [17–28] and measurements [29–31]. While sharing many similarities with discrimination of quantum states, discrimination of quantum devices admits intriguing novel strategies and phenomena [32–38] such as using probes entangled with auxiliary systems, or the perfect distinguishability of any two unitary operations when a sufficiently large but finite number of copies of the operation is available [17].

Here, we investigate the utility of entanglement for the canonical task of optimal discrimination between two projective measurements $\mathcal{M}$ and $\mathcal{N}$ on a single qubit provided that the measurement can be performed only once. We consider general discrimination strategies involving a certain fraction of inconclusive outcomes, P_I, and we show that the optimal discrimination procedure requires entangled probe state unless $P_I = 0$. As a benchmark, we also provide the optimal discrimination scheme with no entanglement. We experimentally implement the optimal discrimination for projective measurements on polarization states of single photons. Our setup is based on linear optics, real-time feed-forward-loop, fiber interferometers, and single-photon detectors. Experimental data unequivocally confirm the advantage of entanglement-based discrimination strategies.

II. OPTIMAL ENTANGLEMENT-ASSISTED DISCRIMINATION

The measurement bases $\mathcal{M}$ and $\mathcal{N}$ are illustrated in Fig. 1(a). Without loss of generality, the projectors specifying the measurements can be parametrized by a single angle θ,

$$M_0 = |\phi\rangle\langle\phi|, \quad M_1 = |\phi^\perp\rangle\langle\phi^\perp|, \\ N_0 = |\psi\rangle\langle\psi|, \quad N_1 = |\psi^\perp\rangle\langle\psi^\perp|, \tag{1}$$

where

$$|\phi\rangle = \cos\theta|0\rangle + \sin\theta|1\rangle, \quad |\phi^\perp\rangle = \sin\theta|0\rangle - \cos\theta|1\rangle, \\ |\psi\rangle = \cos\theta|0\rangle - \sin\theta|1\rangle, \quad |\psi^\perp\rangle = \sin\theta|0\rangle + \cos\theta|1\rangle, \tag{2}$$

and $0 \leqslant \theta \leqslant \frac{\pi}{4}$. The most general discrimination strategy is depicted in Fig. 1(b). A two-qubit entangled state $|\Psi\rangle_{AB}$ is employed, the measurement that should be identified is performed on qubit A, and the measurement outcome (0 or 1) specifies which measurement is then performed on the other qubit B.

In what follows we assume equal *a priori* probabilities of the two measurements. In such a case we will show it is optimal to employ a maximally entangled singlet Bell state $|\Psi^-\rangle = (|01\rangle - |10\rangle)/\sqrt{2}$. If we observe measurement outcome 0 on qubit A, then qubit B is prepared in the state $|\phi^\perp\rangle$ or $|\psi^\perp\rangle$. Similarly, outcome 1 heralds that qubit B is prepared in the state $|\phi\rangle$ or $|\psi\rangle$. The discrimination of quantum measurements is in this way converted to discrimination of two nonorthogonal quantum states. Since

$$|\phi\rangle = -\sigma_Y|\phi^\perp\rangle, \quad |\psi\rangle = \sigma_Y|\psi^\perp\rangle, \tag{3}$$

we can apply the unitary operation $\sigma_Y = |0\rangle\langle 1| - |1\rangle\langle 0|$ to qubit B when the measurement outcome on A reads 0, and we end up with the task to discriminate between two fixed nonorthogonal states $|\phi\rangle$ and $|\psi\rangle$.

As shown by Ivanovic, Dieks, and Peres (IDP) [2], perfect error-free discrimination between $|\phi\rangle$ and $|\psi\rangle$ is possible if we allow for a certain probability of inconclusive outcomes $P_I = |\langle\psi|\phi\rangle|$. Explicitly, we have $P_I = \cos(2\theta)$. Unambiguous discrimination requires a generalized three-component POVM which can be interpreted as a quantum filtering followed by projective measurement on the filtered state. The required filter has the form $F = \tan\theta|0\rangle\langle 0| + |1\rangle\langle 1|$ and the filtered states become orthogonal, $F|\phi\rangle = \sqrt{2}\sin\theta|+\rangle$, and $F|\psi\rangle = \sqrt{2}\sin\theta|-\rangle$, where $|\pm\rangle = (|0\rangle \pm |1\rangle)/\sqrt{2}$. The square of the

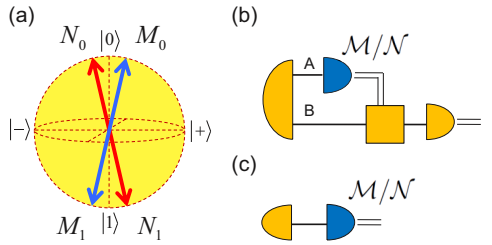

FIG. 1. (Color online) (a) Single-qubit measurements $\mathcal{M}$ and $\mathcal{N}$ on a Bloch sphere. (b) General measurement discrimination scheme involving entangled probe state. (c) Simple discrimination scheme with single-qubit probe.

norm of the filtered states is equal to the success probability of unambiguous discrimination, $P_S = 2\sin^2\theta$, and $P_S + P_I = 1$.

Due to the various experimental imperfections, we will in practice encounter also erroneous conclusive results occurring with probability P_E. This motivates us to consider a general discrimination scheme where we maximize P_S (hence minimize P_E) for a fixed fraction of inconclusive outcomes P_I. The optimal filter then reads $F = f|0\rangle\langle 0| + |1\rangle\langle 1|$, where $f = \sqrt{1 - P_I/\cos^2\theta}$, and a projective measurement in basis $|\pm\rangle$ should be performed after successful filtration similarly as before. This intermediate strategy optimally interpolates between IDP [2] and Helstrom [1] schemes, and we get [4,5]

$$P_S = \frac{1}{2}\left(1 - P_I + \sin(2\theta)\sqrt{1 - \frac{P_I}{\cos^2\theta}}\right). \tag{4}$$

It is convenient to consider also a relative probability of successful discrimination for the subset of conclusive outcomes, $\tilde{P}_S = P_S/(1 - P_I)$. The probability $\tilde{P}_S$ increases with P_I and $\tilde{P}_S = 1$ when $P_I = \cos(2\theta)$.

The optimality of the above protocol can be proved with the help of the formalism of process POVM [32,33]. We associate ith output of the measurement device with quantum state $|i\rangle$, $i = 1,0$, and associate measurement X with operator $E_X = X_0^T \otimes |0\rangle\langle 0| + X_1^T \otimes |1\rangle\langle 1|$, where $X \in \{M,N\}$. An arbitrary test that discriminates between the measurements $\mathcal{M}$ and $\mathcal{N}$ and is allowed by quantum mechanics is described by a three-component process POVM $\{T_M, T_N, T_I\}$ on a Hilbert space of two qubits, where $T_k \geqslant 0$ and $T_M + T_N + T_I = \rho \otimes \mathbb{I}$. Here ρ denotes a density matrix of a single qubit, $\rho \geqslant 0$ and $\mathrm{Tr}[\rho] = 1$, and $\mathbb{I}$ represents an identity operator. Results T_M and T_N correspond to guessing measurement $\mathcal{M}$ and $\mathcal{N}$, respectively, while T_I represents the inconclusive outcomes. Within this formalism, the probabilities P_S, P_E, and P_I can be expressed as follows,

$$\begin{aligned} P_S &= \tfrac{1}{2}\left(\mathrm{Tr}\left[T_M E_M^T\right] + \mathrm{Tr}\left[T_N E_N^T\right]\right), \\ P_E &= \tfrac{1}{2}\left(\mathrm{Tr}\left[T_M E_N^T\right] + \mathrm{Tr}\left[T_N E_M^T\right]\right), \\ P_I &= \tfrac{1}{2}\mathrm{Tr}\left[T_I\left(E_M^T + E_N^T\right)\right]. \end{aligned} \tag{5}$$

Thanks to the block-diagonal structure of E_M and E_N it suffices to consider $T_k = H_{k,0} \otimes |0\rangle\langle 0| + H_{k,1} \otimes |1\rangle\langle 1|$ and the constraint on T_k can be rephrased as

$$H_{M,i} + H_{N,i} + H_{I,i} = \rho, \qquad i = 0,1. \tag{6}$$

Furthermore, due to the property (3) it suffices to consider only covariant T_k, where $H_{k,1} = \sigma_Y H_{k,0}\sigma_Y^\dagger$ and $\rho = \sigma_Y \rho \sigma_Y^\dagger$. This can be seen by noting that the following substitutions do not alter the value of probabilities (5) while making T_k covariant,

$$\begin{aligned} H_{k,0} &\to \tfrac{1}{2}(H_{k,0} + \sigma_Y H_{k,1}\sigma_Y^\dagger), \\ H_{k,1} &\to \tfrac{1}{2}(H_{k,1} + \sigma_Y H_{k,0}\sigma_Y^\dagger). \end{aligned} \tag{7}$$

Finally, since the projectors (1) are real, one can also choose $H_{k,i}$ to be real and set their imaginary parts to zero without changing the probabilities (5). This means that ρ is real as well, which together with $\rho = \sigma_Y \rho \sigma_Y^\dagger$ implies that $\rho = \mathbb{I}/2$. If we combine together all the above results, we find that the probabilities (5) can be expressed as

$$\begin{aligned} P_S &= \mathrm{Tr}[H_{M,0}M_0] + \mathrm{Tr}[H_{N,0}N_0], \\ P_E &= \mathrm{Tr}[H_{N,0}M_0] + \mathrm{Tr}[H_{M,0}N_0], \\ P_I &= \mathrm{Tr}[H_{I,0}(M_0 + N_0)], \end{aligned} \tag{8}$$

and the operators $H_{k,0}$ satisfy the conditions $H_{k,0} \geqslant 0$, and $H_{M,0} + H_{N,0} + H_{I,0} = \mathbb{I}/2$. This shows that the optimization of discrimination of two projective qubit measurements becomes equivalent to optimization of the discrimination of two quantum states M_0 and N_0 by a three-component POVM with elements $2H_{M,0}$, $2H_{N,0}$, and $2H_{I,0}$.

III. OPTIMAL DISCRIMINATION WITH SINGLE-QUBIT PROBES

To elucidate the importance of entanglement for measurement discrimination and to provide a benchmark for the experiment, we now determine the optimal discrimination strategy with unentangled single-qubit probes [see Fig. 1(c)]. In this case one has to guess $\mathcal{M}$ or $\mathcal{N}$ solely based on the measurement outcome on the probe qubit. We shall show that the optimal strategy for a fixed probe state can be constructed such that for observation 0 we always guess $\mathcal{M}$ while for observation 1 we guess $\mathcal{N}$ with probability q and provide an inconclusive outcome with probability $1 - q$. Let ρ denote density matrix of the probe state and define $P_{M,i} = \mathrm{Tr}[M_i\rho]$, $P_{N,i} = \mathrm{Tr}[N_i\rho]$. We can always relabel the measurements and outcomes such that

$$\frac{P_{M,0}}{P_{N,0}} \geqslant \frac{P_{N,1}}{P_{M,1}} \geqslant 1. \tag{9}$$

Note that $P_{M,0} \geqslant P_{N,0}$ implies $P_{N,1} \geqslant P_{M,1}$ because $P_{M,0} + P_{M,1} = P_{N,0} + P_{N,1} = 1$. First observe that it does not help to produce inconclusive outcomes for both observations 0 and 1, because this only increases P_I while not further improving $\tilde{P}_S$ with respect to the strategy where inconclusive results are declared only for outcome 1. The inequalities (9) then imply the optimality of the above defined strategy and we can write

$$\begin{aligned} P_S &= \tfrac{1}{2}(\mathrm{Tr}[M_0\rho] + q\,\mathrm{Tr}[N_1\rho]), \\ P_I &= \tfrac{1}{2}(1 - q)\mathrm{Tr}[(M_1 + N_1)\rho], \end{aligned} \tag{10}$$

and $P_E = 1 - P_S - P_I$. It is easy to verify that for a fixed P_I the probability P_S is maximized when the probe state is pure with real amplitudes, $\rho = |\vartheta\rangle\langle\vartheta|$, where $|\vartheta\rangle = \cos\vartheta|0\rangle +$

$\sin\vartheta|1\rangle$. Explicitly, we get

$$P_S = \frac{1}{2}[1 + \sin(2\theta)\sin(2\vartheta) - (1-q)\sin^2(\theta+\vartheta)],$$
$$P_I = \frac{1-q}{2}(1-cx), \tag{11}$$

where $c = \cos(2\theta)$ and $x = \cos(2\vartheta)$.

Using Eq. (11) we can express q as a function of P_I,

$$q = 1 - \frac{2P_I}{1-xc}. \tag{12}$$

If we insert this formula for q into Eq. (11), we obtain

$$P_S = \frac{1}{2}(1-P_I) + \frac{1}{2}\sqrt{(1-c^2)(1-x^2)}\left[1 - \frac{P_I}{1-xc}\right]. \tag{13}$$

The optimal ϑ that maximizes P_S for a given P_I can be determined from the condition,

$$\frac{\partial P_S}{\partial x} = 0, \tag{14}$$

which leads to a qubic equation for x,

$$c^2x^3 - 2cx^2 + (1-P_I)x + P_Ic = 0. \tag{15}$$

This construction is applicable only if $q > 0$, which is equivalent to $P_I < P_{I,B}$, where the boundary $P_{I,B}$ can be determined from the condition that x satisfies Eq. (15) and, simultaneously, $q = 0$. After some algebra, this yields a quadratic equation $8P_{I,B}^2 - 6P_{I,B} + 1 - c^2 = 0$, whose solution reads

$$P_{I,B} = \tfrac{1}{8}\left(3 + \sqrt{1+8c^2}\right), \tag{16}$$

If $P_I \geqslant P_{I,B}$, then it is optimal to set $q = 0$. This implies $x = (1-2P_I)/c$ and

$$P_S = \frac{1}{2}(1-P_I) + \frac{1}{4}\sin(2\theta)\sqrt{1 - \frac{(1-2P_I)^2}{\cos^2(2\theta)}}. \tag{17}$$

Explicit numerical calculations reveal that the resulting dependence of P_S on P_I is a convex function for $P_I < P_{I,B}$ (see the appendix). Equation (13) therefore does not determine the optimal discrimination strategy with single-qubit probes. The situation is depicted in Fig. 2. The blue crosses represent the dependence of P_S on P_I specified by Eqs. (13) and (17). Since P_S is a convex function of P_I for $P_I < P_{I,B}$, the area below the curve $P_S(P_I)$ does not form a convex set.

In order to obtain the optimal discrimination strategy with single-qubit probes, we must construct a convex hull of the discrimination strategies represented by blue crosses in Fig. 2. The result is indicated by red circles. Geometrically, we must construct a tangent line to the curve specified by Eq. (17), which passes through the point A that corresponds to the optimal minimum error discrimination: $\vartheta = \pi/4$, $P_{I,0} = 0$, $P_{S,0} = [1 + \sin(2\theta)]/2$. This tangent line touches the curve (17) at point T, which is specified by

$$P_{I,T} = \frac{1 + 3c^2 + 2c^2\sqrt{1+3c^2}}{2(1+4c^2)}. \tag{18}$$

Note that $P_{I,T} \geqslant P_{I,B}$. In the interval $0 < P_I < P_{I,T}$ the optimal discrimination strategy is thus a mixture of two

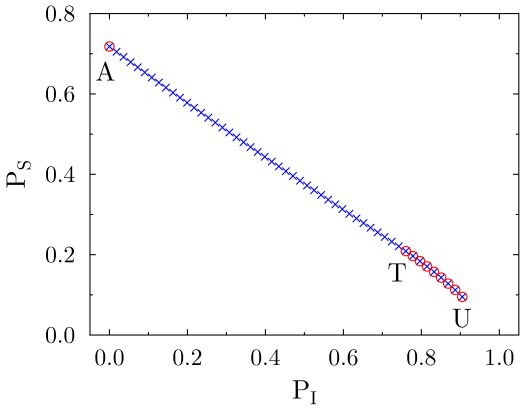

FIG. 2. (Color online) Blue crosses show the dependence of P_S on P_I as specified by Eqs. (13) and (17); $c = 0.9$. The red circles indicate the convex hull, points A and U correspond to minimum error and unambiguous discrimination with single-qubit probes, respectively, and point T is specified by Eq. (18).

strategies corresponding to points A and T with weights $1 - P_I/P_{I,T}$ and $P_I/P_{I,T}$, respectively. This means that with probability $1 - P_I/P_{I,T}$ we should perform the optimal minimum-error discrimination with probe state $|\vartheta\rangle = |+\rangle$ and $q = 1$, which results in $P_{S,0} = [1 + \sin(2\theta)]/2$ and $P_{I,0} = 0$. With probability $P_I/P_{I,T}$ we should use the probe state with $x = (1-2P_{I,T})/c$, which yields $P_S = P_{S,T}$ given by Eq. (17), where P_I is replaced with $P_{I,T}$. The overall success probability then reads

$$P_S = \left(1 - \frac{P_I}{P_{I,T}}\right)P_{S,0} + \frac{P_I}{P_{I,T}}P_{S,T}. \tag{19}$$

If $P_I \geqslant P_{I,T}$, then it is optimal to use only one single-qubit probe specified by $x = (1-2P_I)/c$. In this case, the optimal P_S is given by Eq. (17); see also the red circles in Fig. 2. The endpoint U corresponds to unambiguous discrimination with a single-qubit probe: $\vartheta = \pi/2 - \theta$, $P_S = (1-c^2)/2$, and $P_I = (1+c^2)/2$.

To verify the validity of our analytical construction, we have performed extensive numerical analysis of the convex hulls for various values of c using the MATLAB function convhull. For each chosen c, we have generated 10^4 pairs (P_I, P_S) corresponding to discrimination strategies described by Eqs. (13) and (17), and we have numerically calculated the convex hull. In all cases, the convex hull constructed in this way had the structure illustrated in Fig. 2 and the position of point T agreed with the analytical formula (18).

IV. EXPERIMENT

Our experimental demonstration of entanglement-assisted discrimination of quantum measurements is based on linear optics and qubits encoded into states of single photons. The scheme of our experimental setup is shown in Fig. 3. Time-correlated orthogonally polarized photon pairs were generated by the process of collinear frequency-degenerate type-II spontaneous parametric down-conversion in a 2-mm-thick BBO crystal pumped by a continuous wave laser diode at 405 nm. A postselected two-photon polarization singlet Bell state $|\Psi^-\rangle$ was prepared by interfering the vertically polarized

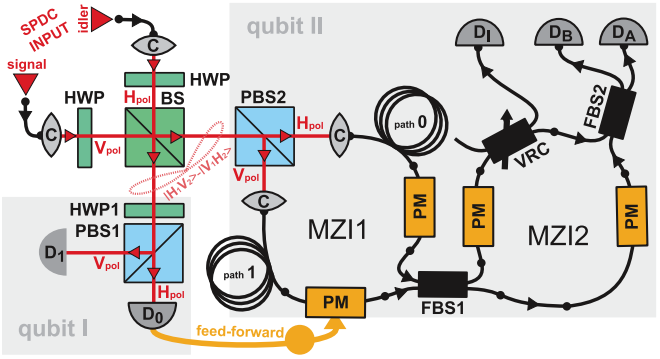

FIG. 3. (Color online) The scheme of the experimental setup. Bulk beam splitter (BS) 50:50; fiber beam splitter (FBS) 50:50; polarizing beam splitter (PBS); half-wave plate (HWP); collimating lens (C), phase modulator (PM), and single-photon detector (D).

signal photon and horizontally polarized idler photon at a balanced beam splitter (BS). The state was characterized by quantum state tomography and we observed purity >98% and fidelity >99%.

In the main experiment, the measurement that should be identified was performed on the first photon of the entangled pair $|\Psi^-\rangle$. The measurement basis ($\mathcal{M}$ or $\mathcal{N}$) was set by rotating a half-wave plate HWP1 in front of the polarizing beam splitter PBS1. We associated the basis states $|0\rangle$ and $|1\rangle$ with diagonal $|D\rangle$ and antidiagonal $|A\rangle$ linear polarizations, respectively. Namely, $|\phi\rangle = \cos\theta|D\rangle + \sin\theta|A\rangle$ and similarly for other measurement-basis states. Measurement outcomes 0 and 1 were indicated by clicks of detectors D_0 and D_1, respectively. The polarization state of the second photon was transformed to path encoding with the help of PBS2 and the photon was coupled into the first of two serially connected fiber-based Mach-Zehnder interferometers (MZI1). Thus, polarization states $|V\rangle = (|D\rangle + |A\rangle)/\sqrt{2} \equiv |+\rangle$ and $|H\rangle = (|D\rangle - |A\rangle)/\sqrt{2} \equiv |-\rangle$ were then represented by a photon propagating in the lower and upper interferometer arm, respectively. We employed polarization maintaining fibers which suppressed unwanted changes of the photon's polarization state during its propagation in the fibers. Both interferometers MZI1 and MZI2 were thermally isolated and actively stabilized to reduce phase drifts caused by temperature fluctuations and air flux. If detector D_0 registered a photon then an electronic feed-forward [39] conditionally changed the state of the second photon in MZI1 by applying a π-phase shift in the lower interferometer arm. This resulted in transformation $|\phi^\perp\rangle \to |\psi\rangle$ and $|\psi^\perp\rangle \to |\phi\rangle$ which is equivalent to the conditional application of unitary operation σ_Y in Eq. (3) up to an exchange of the role of $|\phi\rangle$ and $|\psi\rangle$.

The discrimination problem was thus reduced to a discrimination between two single-qubit states $|\phi\rangle$ and $|\psi\rangle$. Behind the balanced fiber coupler FBS1 propagation of a photon through the upper (lower) arm corresponded to the state $|0\rangle$ ($|1\rangle$). A variable-ratio coupler (VRC) placed in the upper arm of MZI2 was used as a variable attenuator of the amplitude of the basis state $|0\rangle$, hence it implemented the filter F. Projection onto the superposition states $|\pm\rangle$ was achieved using the final balanced fiber coupler FBS2 and detectors D_A and D_B. To determine the probability of inconclusive events, additional detector D_I was used to monitor the output of the tunable fiber coupler VRC. For each basis $X = M, N$ we have measured six two-photon coincidences C_{ik}^X represented by simultaneous clicks of pairs of detectors D_i and D_k, where $i = 0,1$, and $k = A, B, I$. We had measured the relative detection efficiencies η_i, η_k of the detectors, and their influence was compensated by rescaling the measured coincidence rates as $C_{ik}^X \to C_{ik}^X/(\eta_i\eta_k)$. The measurement time was the same for both bases which corresponds to equal *a priori* probabilities of $\mathcal{M}$ and $\mathcal{N}$. The probabilities P_S and P_I were then determined as $P_S = (C_{0A}^M + C_{1B}^M + C_{1A}^N + C_{0B}^N)/C_{\rm tot}$ and $P_I = (C_{0I}^M + C_{1I}^M + C_{0I}^N + C_{1I}^N)/C_{\rm tot}$, where $C_{\rm tot}$ denotes the sum of all 12 measured coincidence rates.

V. RESULTS

We have performed measurements for seven values of $\theta = j\pi/30$, $j = 1,2,3,4,5,6,7$. For each fixed θ, the transmittance of VRC was varied from 1 to 0.1 with the step of 0.1. The resulting dependence of $\tilde{P}_S$ on P_I is plotted in Fig. 4 by circles together with the theoretical curves representing the maximum $\tilde{P}_S$ achievable by the optimal entanglement-assisted protocol (solid lines) and by using the single-qubit probes (dashed lines). The statistical errors of the results are smaller than the size of the symbols. We can see that for certain θ and P_I the experimental entanglement-based discrimination indeed outperforms the best strategy without entanglement. The slight reduction of the experimentally observed $\tilde{P}_S$ with respect to the theoretical prediction could be attributed to various experimental imperfections such as phase fluctuations inside MZIs, arm disbalance, slight deviations in phase and polarization settings, slightly unbalanced splitting ratios of beam splitters, and small imperfections in the input singlet state. As indicated by the theoretical curves, the entanglement-

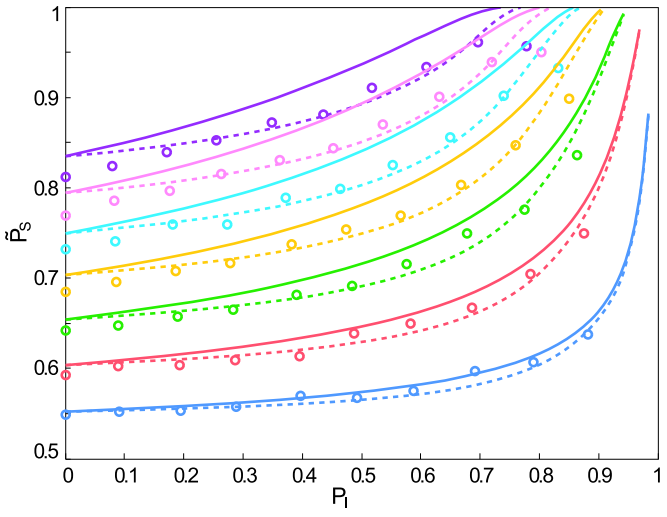

FIG. 4. (Color online) Dependence of relative success probability $\tilde{P}_S$ on probability of inconclusive results P_I is plotted for seven values of $\theta_j = j\pi/30$, $j = 1,2,3,4,5,6,7$. The value of j increases from bottom to top. Shown are the experimental data (circles) as well as the maximum $\tilde{P}_S$ achievable by the optimal scheme using entangled state (solid lines), and using single-qubit probes only (dashed lines).

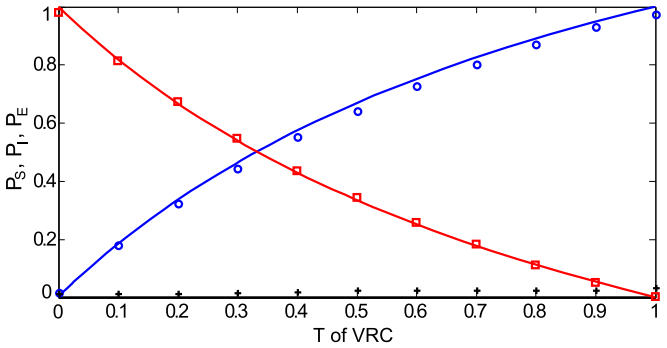

FIG. 5. (Color online) Unambiguous discrimination of quantum measurements. The probabilities P_S (blue circles), P_I (red squares), and P_E (black crosses) are plotted as functions of the VRC splitting ratio T. The lines represent theoretical predictions.

based protocol in theory outperforms the single-qubit scheme for all $P_I > 0$. The entanglement thus does not help only in the regime of minimum error discrimination ($P_I = 0$) where the optimal success probability $[1 + \sin(2\theta)]/2$ can be achieved by a single-qubit probe prepared in state $|+\rangle$. Unambiguous discrimination with the single-qubit probe is possible only if the probe is prepared in a state orthogonal to one of the projectors (1), say $|\vartheta\rangle = |\psi^{\perp}\rangle$. The resulting probability of inconclusive outcomes $P_I = [1 + \cos^2(2\theta)]/2$ is larger than the probability $\cos(2\theta)$ achieved by the entanglement-based scheme and the difference increases with θ. We have carried a separate test of unambiguous discrimination for 11 different $\theta_j = \arctan(\sqrt{T_j})$ corresponding to transmittances of the VRC, T_j, varied from 0 to 1 with step 0.1. The experimental results, plotted in Fig. 5, are in good agreement with theory and the probability of errors P_E does not exceed 3.2%.

VI. CONCLUSIONS

In summary, we have determined theoretically and implemented experimentally optimal strategies for discrimination between two projective single-qubit quantum measurements. The experiment demonstrates that the quantum optical technology is mature enough to harness the benefits of entanglement in quantum device discrimination, although the entanglement-based scheme is much more demanding than the single-qubit probe scheme, as the former requires a real-time feed-forward to fully exploit the potential of entangled probes. The techniques and results reported here can be extended to unequal *a priori* probabilities of $\mathcal{M}$ and $\mathcal{N}$, noisy measurements, and POVMs containing more than two elements [40]. Our findings provide fundamental insight into the structure of optimal probabilistic discrimination schemes for quantum measurements and they pave the way towards potential applications of such techniques in quantum information science and beyond.

ACKNOWLEDGMENTS

This work was supported by the Czech Science Foundation (Grant No. GA13-20319S). M.S. acknowledges support by the Operational Program Education for Competitiveness—European Social Fund (Project No. CZ.1.07/2.3.00/30.0004) of the Ministry of Education, Youth and Sports of the Czech Republic. M.Z. acknowledges the support of projects VEGA 2/0125/13 (QUICOST), COST Action MP 1006, and APVV-0646-10 (COQI). M.M. and I.S. acknowledge support by the Palacký University (Grant No. IGA_PrF_2014008).

APPENDIX: PROPERTIES OF P_S IN THE PROTOCOL WITH SINGLE-QUBIT PROBES

Here we discuss in detail the properties of the probability of successful discrimination P_S in a scenario where the two projective single-qubit measurements are discriminated using one pure single-qubit probe. In particular, we prove that the success probability P_S given by Eq. (13) is a convex function of P_I on the entire interval $0 < P_I < P_{I,B}$, i.e.,

$$\frac{d^2 P_S}{dP_I^2} > 0. \tag{A1}$$

It is convenient to introduce a new variable $y = cx$. It follows from Eq. (15) that y is a root of a cubic equation,

$$y^3 - 2y^2 + (1 - P_I)y + P_I c^2 = 0, \tag{A2}$$

which defines y as an implicit function of P_I. If we make the substitution $x = y/c$ in Eq. (13) we get

$$P_S = \frac{1}{2}(1 - P_I) + \frac{\sqrt{1 - c^2}}{2c}\sqrt{c^2 - y^2}\left[1 - \frac{P_I}{1 - y}\right], \tag{A3}$$

where y depends on P_I through Eq. (A2).

After some algebra we arrive at

$$\frac{d^2 P_S}{dP_I^2} = \frac{\sqrt{1 - c^2}}{2c}(\alpha y' + \beta y'^2 + \gamma y''), \tag{A4}$$

where

$$y' = \frac{dy}{dP_I}, \qquad y'' = \frac{d^2 y}{dP_I^2}, \tag{A5}$$

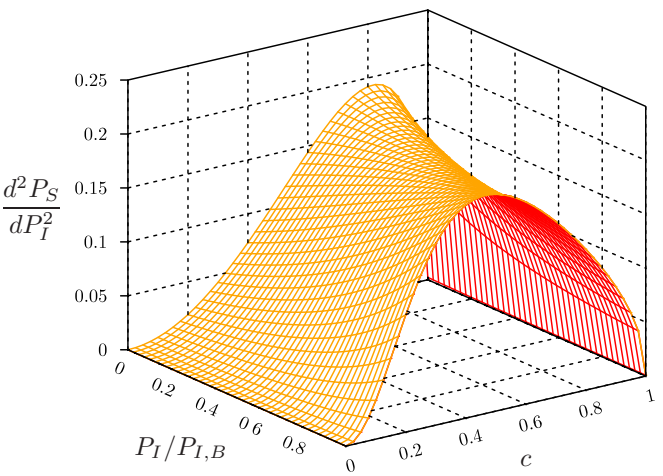

FIG. 6. (Color online) The second derivative $d^2 P_S/dP_I^2$ given by Eq. (A4) is plotted as a function of P_I and c.

and

$$\alpha = \frac{2(y-c^2)}{\sqrt{c^2-y^2}(1-y)^2}, \quad \beta = \frac{P_I(3c^2y^2+c^2-2c^4-2y^3)-c^2(1-y)^3}{(c^2-y^2)^{3/2}(1-y)^3}, \quad \gamma = \frac{(y-c^2)P_I}{\sqrt{c^2-y^2}(1-y)^2} - \frac{y}{\sqrt{c^2-y^2}}. \tag{A6}$$

The derivatives y' and y'' can be determined by repeatedly differentiating Eq. (A2) with respect to P_I, which yields

$$y' = \frac{y-c^2}{3y^2-4y+1-P_I}, \tag{A7}$$

$$y'' = 2\frac{y'+y'^2(2-3y)}{3y^2-4y+1-P_I}. \tag{A8}$$

When evaluating the second derivative (A4), we should use the root of the cubic equation (A2) which maximizes the probability of success (A3). The dependence of $\frac{d^2P_S}{dP_I^2}$ on P_I and c is plotted in Fig. 6. We can see that the second derivative is non-negative for all $0 \leqslant c \leqslant 1$ and $0 \leqslant P_I \leqslant P_{I,B}$.

When $P_I > P_{I,B}$, then it is optimal to set $q = 0$ and P_S is given by Eq. (17), which is a concave function of P_I. In this case the second derivative can be explicitly calculated, and we get

$$\frac{d^2P_S}{dP_I^2} = -c\sqrt{1-c^2}[c^2-(1-2P_I)^2]^{-3/2} < 0. \tag{A9}$$

[1] C. W. Helstrom, *Quantum Detection and Estimation Theory* (Academic Press, New York, 1976).
[2] I. D. Ivanovic, Phys. Lett. A **123**, 257 (1987); D. Dieks, *ibid.* **126**, 303 (1988); A. Peres, *ibid.* **128**, 19 (1988).
[3] G. Jaeger and A. Shimony, Phys. Lett. A **197**, 83 (1995).
[4] A. Chefles and S. M. Barnett, J. Mod. Opt. **45**, 1295 (1998).
[5] C. W. Zhang, C. F. Li, and G. C. Guo, Phys. Lett. A **261**, 25 (1999).
[6] J. Fiurášek and M. Ježek, Phys. Rev. A **67**, 012321 (2003).
[7] A. Hayashi, T. Hashimoto, and M. Horibe, Phys. Rev. A **78**, 012333 (2008).
[8] H. Sugimoto, T. Hashimoto, M. Horibe, and A. Hayashi, Phys. Rev. A **80**, 052322 (2009).
[9] E. Bagan, R. Muñoz-Tapia, G. A. Olivares-Rentería, and J. A. Bergou, Phys. Rev. A **86**, 040303 (2012).
[10] M. Dušek, M. Jahma, and N. Lütkenhaus, Phys. Rev. A **62**, 022306 (2000).
[11] M. Dušek and V. Bužek, Phys. Rev. A **66**, 022112 (2002).
[12] B. Huttner, A. Muller, J. D. Gautier, H. Zbinden, and N. Gisin, Phys. Rev. A **54**, 3783 (1996).
[13] S. M. Barnett and E. Riis, J. Mod. Opt. **44**, 1061 (1997).
[14] R. B. M. Clarke, A. Chefles, S. M. Barnett, and E. Riis, Phys. Rev. A **63**, 040305 (2001).
[15] L. Bartůšková, A. Černoch, J. Soubusta, and M. Dušek, Phys. Rev. A **77**, 034306 (2008).
[16] J. Soubusta, A. Černoch, J. Fiurášek, and M. Dušek, Phys. Rev. A **69**, 052321 (2004).
[17] A. Acin, Phys. Rev. Lett. **87**, 177901 (2001).
[18] G. M. D'Ariano, P. Lo Presti, and M. G. A. Paris, Phys. Rev. Lett. **87**, 270404 (2001).
[19] M. F. Sacchi, Phys. Rev. A **71**, 062340 (2005).
[20] G. Wang and M. Ying, Phys. Rev. A **73**, 042301 (2006).
[21] R. Duan, Y. Feng, and M. Ying, Phys. Rev. Lett. **103**, 210501 (2009).
[22] M. Piani and J. Watrous, Phys. Rev. Lett. **102**, 250501 (2009).
[23] A. W. Harrow, A. Hassidim, D. W. Leung, and J. Watrous, Phys. Rev. A **81**, 032339 (2010).
[24] M. Ziman and M. Sedlák, J. Mod. Opt. **57**, 253 (2010).
[25] T. Hashimoto, A. Hayashi, M. Hayashi, and M. Horibe, Phys. Rev. A **81**, 062327 (2010).
[26] A. Laing, T. Rudolph, and J. L. O'Brien, Phys. Rev. Lett. **102**, 160502 (2009).
[27] P. Zhang, L. Peng, Z. W. Wang, X. F. Ren, B. H. Liu, Y. F. Huang, and G. C. Guo, J. Phys. B: At. Mol. Opt. Phys. **41**, 195501 (2008).
[28] M. Dall'Arno, A. Bisio, G. M. D'Ariano, M. Miková, M. Ježek, and M. Dušek, Phys. Rev. A **85**, 012308 (2012).
[29] M. Ziman and T. Heinosaari, Phys. Rev. A **77**, 042321 (2008).
[30] Z. Ji, Y. Feng, R. Duan, and M. Ying, Phys. Rev. Lett. **96**, 200401 (2006).
[31] J. Fiurášek and M. Mičuda, Phys. Rev. A **80**, 042312 (2009).
[32] M. Ziman, Phys. Rev. A **77**, 062112 (2008).
[33] G. Chiribella, G. M. D'Ariano, and P. Perinotti, Phys. Rev. Lett. **101**, 180501 (2008).
[34] G. Chiribella, G. M. D'Ariano, and P. Perinotti, Phys. Rev. Lett. **101**, 060401 (2008).
[35] G. Chiribella, G. M. D'Ariano, and P. Perinotti, Europhys. Lett. **83**, 30004 (2008).
[36] G. Chiribella, G. M. D'Ariano, and P. Perinotti, Phys. Rev. A **80**, 022339 (2009).
[37] G. Gutoski and J. Watrous, in *Proceedings of the 39th Annual ACM Symposium on Theory of Computation* (ACM, New York, 2007), pp. 565–574.
[38] G. Chiribella, G. M. D'Ariano, and M. Roetteler, New J. Phys. **15**, 103019 (2013).
[39] M. Miková, H. Fikerová, I. Straka, M. Mičuda, J. Fiurášek, M. Ježek, and M. Dušek, Phys. Rev. A **85**, 012305 (2012).
[40] M. Sedlák and M. Ziman, arXiv:1408.0934.